DEMONSTRATING THE IMPORTANCE OF EMISSIVITY MEASUREMENT IN DETERMINING THE DOSES OF LIGHT SOURCES ON TISSUE MIMICKING MATERIALS SUCH AS LASER, IPL AND LED

HÜSEYIN OKAN DURMUŞ[1,2], MIRHASAN Yu SEYIDOV[1]
[1]Department of Physics, Gebze Technical University, 41400, Kocaeli, Turkey
[2]Medical Metrology Laboratory, TUBITAK National Metrology Institute (TUBITAK UME), 41470, Kocaeli, Turkey
E-mail: hokandurmus@gtu.edu.tr, smirhasan@gtu.edu.tr;
Tel : (262) 605 10 00; Fax: (262) 653 84 90

Nowadays, a wide variety of low-power light sources such as IPL, LED and laser are frequently used in therapy applications. In this study, irradiance values were calculated for different emissivity values by using the temperature measurement results made in the agar phantom using low-power light sources such as LED, IPL and laser. Based on the irradiance data, energy densities (J/cm^2) as per the different emissivity coefficient and time durations are calculated and the results were evaluated in terms of dose quantities given in the literature. We also present in detail both acoustic and optical characterization of the agar phantom. In conclusion, we clearly show the importance of emissivity measurement in this study. Our findings explicitly suggest that emissivity measurement must be determined precisely to determine optical power density and/or energy density values and hence doses can be applied on the base of this values.

Keywords. Temperature Measurement, Emissivty, Irradiance, Energy Density, Dose, Low-Power Light Sources, Laser, IPL, LED.
DOI: https://doi.org/10.21203/rs.3.rs-1557976/v1

INTRODUCTION

In recent years, the use of light therapy in the field of health has been expanding. These low-light-intensity therapies are called as photobiomodulation therapy. Photobiomodulation therapy (PBMT) mainly includes low-level laser therapy (LLLT), light-emitting diode (LED) therapy, and broadband light therapy (IPL-Intense Pulsed Light) [1]. Discovered in the late 1960s, this treatment is also called as cold laser, soft laser, low-intensity laser and biostimulatory laser therapy. PBMT is different from lasers that destroy or cut tissue used in cosmetic and surgical procedures.

PBMT, on the other hand, employs non-ionizing, non-thermal light sources in the visible and infrared spectrum (600-1200 nm) to decrease inflammation and promote healing. The light is directed at injured or inflamed tissues through the skin. Intracellular photoreceptors absorb light energy, which triggers a sequence of photochemical intracellular reactions that boost cellular activity and speed up tissue repair. PBMT is also cost-effective, non-invasive, and has been shown to have no negative side effects [2,3,4]. PBM is a treatment used by irradiation with light at low power density. As used at optimum condition of wavelengths and fluences, the beneficial effects of PBMT are photochemical, not thermal because they have been often resulted from the photostimulation of the mitochondrial electron transfer chain. PBMT not only produces therapeutic effects, but also causes no adverse effects on target organs. [4].

PBMT is used to stimulate, heal and regenerate damaged tissue and is thought to work best on diseased or damaged tissue [3]. PBMT has recently been used to treat thousands of individuals all over the world for a variety of medical and dermatological disorders. Applications of PBMT for aesthetic therapy of disorders such as scars, fine wrinkles, inflammatory acne, photoaged skin, and others have gotten a lot of attention in the recent several decades. PBMT has also been proven to have the ability to improve various dermatological disorders such as acne, vitiligo, and hair loss, as well as cellulite therapy and tooth whitening [4]. It is reported in the literature that PBMT effectively and successfully cures many health problems such as ulcer healing treatment [5-8], wound healing [9-11], tissue repair [12,13], acne vulgaris treatment [14,15], laser hair reduction [16] and skin rejuvenation [17] operations, in improving symptoms of ocular discomfort such as dry eye problem [18] and enhancing bone repair and accelerating bone healing [1]. Furthermore, PBMT has been reported to be an adjuvant therapy option for pain management, lymphedema, wound healing, and musculoskeletal problems [2].

In this study, we present the irradiance and energy density values we calculated on the base of internal temperatures data caused by low power IPL, LED and laser light sources within the agar phantom, with respect to different emissivity coefficients, and we discuss the importance of emissivity coefficient. We also demonstrate optical and acoustial characterization study of the agar phantom. Lastly, we evaluate treatment application times of the investigated light sources, as per the given energy densities for the treatment of various diseases with light in the literature.

METHODOLOGY

In this study, agar phantom, LED, IPL and laser devices and various types of thermocouples were used. All experiments were performed under controlled laboratory ambient conditions.

131, H.Javid ave, AZ-1143, Baku
ANAS, Institute of Physics
E-mail: jophphysics@gmail.com

PREPARATION OF AGAR PHANTOM

Tissue phantom or Tissue-Mimicking Material (TMM) is a kind of material widely applied in medical ultrasonic studies and research due to its capability to mimic biological soft tissues. In our research, as a tissue phantom, agar material was used. Agar phantom was made by preparing approximately a 250 ml solution with 0.4 M ZnCl2 and 2 % Agar by the weight of the initial water [19].

THE LIGHT EQUIPMENTS AND MEASUREMENT SYSTEMS

Philips brand, Lumea Prestige model IPL (epilation) device, Tristar One brand LED therapy device and Optotronics branded VA-I-400-635 model 635 nm wavelength red colored solid-state diode laser were used in the experiments. The laser, IPL and LED devices used on the agar phantom in the experiments can be seen in Figure 1. The operating range of the devices was as follows. The operating range of IPL device was between 560 nm and 1200 nm. The LED therapy device has 110 LEDs on its right side, 110 LEDs on its left side and 110 LEDs on the top, with four basic lights. These LEDs were mainly red, green, blue and yellow in colour. Red LED was operating at 640 nm wavelength, Blue LED was operating at 423 nm wavelength, Green LED was operating at 532 nm wavelength and Yellow LED was operating at 583 nm wavelength. Maximum working power of the 635 nm red color laser was 400 mW. T-type ultra-fine thermocouples (Physitemp, accuracy is ±0.04 °C) were placed at 15 mm depth in from the phantom surface for the IPL and laser temperature measurement studies. The distance between the four thermocouples was set to be as 2 mm apart. In the LED research, four pieces T-Type Metronik commercial thermocouple with an accuracy of 0.2 °C were used as a thermocouple within the phantom. A PC-based Data Acquisition and Monitoring Interface system was used for multi-channel temperature measurements within the phantom [20-22].

Fig. 1. (a) Laser, b) IPL, and (c) LED devices used in the temperature measurement experiments.

THE EMISSIVITY, IRRADIANCE AND DOSE CONCEPT

The efficiency with which a material emits or absorbs energy is referred to as emissivity. The emissivity values are all in the range of 0.0 to 1.0. Because it is expressed as a perfect emitter, The emissivity rating of 1.0 means that 100% of the energy is emitted. A 0.0 emissivity value indicates that the object does not emit any radiation. Materials with a high emissivity value are extremely reflecting or brilliant, whereas materials with a low emissivity value are dark and dull. Emissivity is a complicated material attribute that is influenced by a variety of factors, including material type, surface structure, geometry, observation direction, wavelength, and temperature. The material is the most important factor. Materials can be separated into metal and nonmetal categories in a simplistic categorization. Skin, paper, glass, polymer, and other nonmetallic materials utilized in thermography can be classified as gray bodies and have an emissivity of greater than 0.8. Metallic materials, especially polished metals, on the other hand, often have an emissivity of less than 0.2. Even for the same material, the surface structure can have a significant impact on its emissivity. For instance, a polished metal can have an emissivity of 0.02, but if the surface is roughened, the number rises to almost 0.8 [23].

The Stefan-Boltzmann law, as shown in Eq.1-3, says that thermal radiation intensity depends on the fourth power of the temperature.

$$I = e\sigma T^4 \quad \text{[24] (1)}$$

$$I = \frac{P}{A} \quad (2)$$

$$P = e\sigma A T^4 \quad (3)$$

In the equations, “I” represents the intensity of the radiation or the power per unit area, “e” represents the object's surface radiation emissivity coefficient, which is a dimensionless number between 0 and 1, “σ” is the Stefan-Boltzmann constant (σ= 5,6703 x 10^{-8} Watt m^{-2} K^{-4}), “T” represents the temperature, “P” represents the power, and “A” represents the area of the cavity opening.

The light dose is evaluated using the following formula;

Dose = (Power Density x Time) x 0.001 [25] (4)

The same standardized units and measurements (doses as J/cm², power density as mW/cm², and also time as seconds (s) unit) are utilized when computing the light doses.

THE OPTİCAL CHARACTERİZATİON SETUP

Optical equipment included a compact spectrometer (Thorlabs, CCS200/M) with a wavelength range of 200 nm to 1000 nm, a broadband stabilized fiber-coupled white light source (Thorlabs, SLS201L/M), and a single integrating sphere (Thorlabs IS200 type 2" integrating sphere). And the thickness of the agar phantom specimen cut out as a sample was 22 mm. Figure 1 shows the experiment set-up, and Figure 2 shows how all of the optical measurements and computations were realized using Thorlabs OSA software.

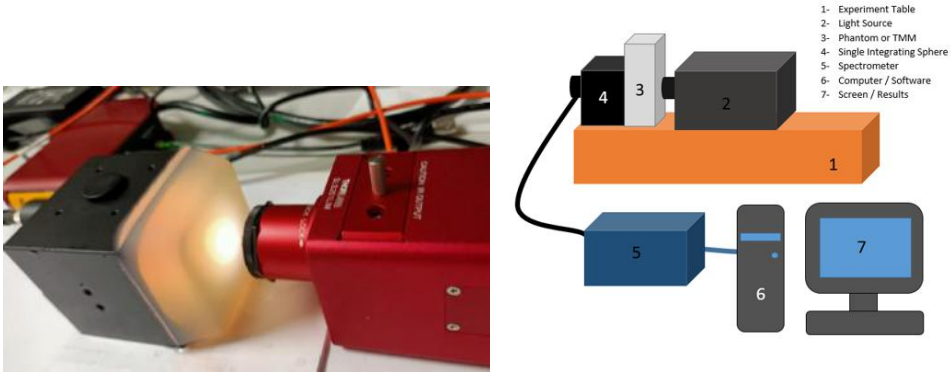

a) b)

Fig. 2. a) A picture showing the phantom measurement; b) Experiment set-up. 1-experimental table, 2-light source, 3-sample (phantom or TMM), 4-single integrating sphere, 5-compact spectrometer, 6-computer and 7-computer monitor.

ASSESSMENT OF THE OPTİCAL DATA

First, the spectrum of the incoming light was obtained during the measurement. The light spectrum was received in the absence of the phantom material in the experimental setup for this. To remove the background noise in the dark environment, the same procedure was applied. The primary signal was then taken by subtracting the dark from the light. The phantom was then placed to the system, and the phantom's spectrum was recorded. The dark, which is background noise, was then eliminated to produce the real phantom signal. The "I_0" data is represented by the main signal, while the "I" signal is represented by the real phantom signal. As a consequence, the following given formulas were used to extract macroscopic and microscopic optical characteristics from the acquired Main Signal (Light-Dark) and Real Phantom (Phantom-Dark) data.

CALCULATION OF OPTICAL PROPERTIES

Optical properties such as absorbance, transmittance, reflectance, the refractive index, and optical attenuation coefficient were measured and calculated by using the following formulas.

R+T+A =1 or%R+%T+%A = %100 [26] (5)

Absorbance, A;

A=-log(I/I0)=-log(T)=2-log(%T) [27] (6)

Transmittance, T; T = I/I0 [27] (7)

Reflectance, R; R=1-(A+T) [26] (8)

$$\text{Reflectance, } R = \frac{(n-1)^2}{(n+1)^2}, \quad [26]\ (9)$$

where n is the Refractive Index.

$$I = I_0 e^{-\mu x},\ \mu = -\frac{\ln \frac{I}{I_0}}{x} \quad [28]\ (10)$$

Where μ is the Linear Attenuation Coefficient.

The related microscopic formulas used in the calculations for absorption coefficient, scattering coefficient, reduced scattering coefficient, and total attenuation coefficient are as in the following.

The Kubelka-Munk Function is given by

$$F(R) = \frac{(1-R)^2}{2R} = \frac{k}{s} \quad [29]\ (11)$$

where R = Reflectance, k= Absorption Coefficient, s=Scattering Coefficient.

The total attenuation coefficient is described by

$$\mu = \mu_t = \mu_a + \mu_s \quad [30]\ (12)$$

Where μ_a is Absorption Coefficient and μ_s is Scattering Coefficient.

That is, k=μ_a and s=μ_s can be matched by using (11) and (12) formulas.

The reduced scattering coefficient (μ_s') is defined by the following equation;

$$\mu_s' = (1-g)\mu_s \quad [31] \quad (13)$$

Where g is the anisotropy factor. The g value of the phantom was used as 0.98 for the agar phantom.

RESULTS AND DISCUSSION

First of all, we give the optical and acoustic characterization results of the agar phantom to show that the agar phantom used in the experiments has real tissue properties. The phantom's tissue-mimicking features were validated acoustically. The sound speed was measured as 1606,78 ± 13 m/s. Attenuation coefficient was measured as 0.60 ± 0.05 dB·cm^{-1}·MHz^{-1}. And acoustic impedance was 1.70 MRayl. According to Mast's study [32], a liver tissue has the speed of sound as 1595 m/s. As seen, agar phantom has a liver-tissue characteristics. The macroscopic and microscopic optical properties of agar phantom were investigated using a spectrometer with a single integrated sphere and a broadband white light source in the wavelength range of 200 nm to 1000 nm. In fact, spectras were originally taken between 200 nm and 1000 nm. However, since the resolution of the signals was very high, the noise level was also very high. Moving average of the data was taken to reduce the noise level and get more smoother signals. For this reason, the absorption spectrum range, shown in the Figure 3, was obtained between 400 nm and 1000 nm. All the experiments done for optical measurements were carried out under controlled laboratory ambient conditions (Temperature was 23.5 °C ± 0.2 °C, and Relative Humidity (RH) was 50% ± 2%). In all graphs of repeated experiments, the individual maximum points were found and the average peak values were calculated. Then, using the absorbance values at the peak values in each measurement, all other optical parameters were calculated for this peak value using the formulations given above. By using these macroscopic optical properties, microscopic optical properties such as absorption coefficient, scattering coefficient, reduced scattering coefficient and total attenuation coefficient were calculated via Kubelka-Munk Function approach. We calculated the total attenuation coefficient from formula (10) and we know R = reflectance value, then we can solve these two equation (11) and (12) and find absorption and scattering coefficients. By the way, while calculating reduced scattering coefficient, we used 0.98 value for the agar phantom. The absorbance peak values we found for the agar phantom were in the range of 645.55 ± 61.05 nm and the absorption coefficient was found to be 0.050 ± 0.008 mm^{-1}. This value is in good agreement with the absorption coefficient values given in the literature [33].

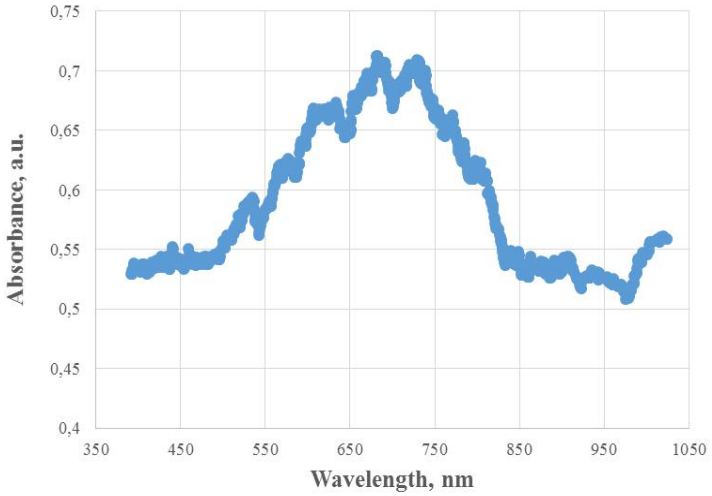

Fig. 3. Absorbance Spectrum of Agar Phantom.

The macroscopic optical properties of agar phantom such as absorbance, transmittance, reflectance, refractive index and attenuation coefficient, which was subtracted from the formulas at the peak values, were calculated as average in the Table I.

Table I.

The measured optical properties of the agar phantom as average

Phantom	Transmittance T	Absorbance A	Reflectance R	Refractive Index
Agar	0.23 ± 0.03	0.64 ± 0.06	0.13 ± 0.03	2.14 ± 0.18

The microscopic optical properties of agar phantom such as absorption coefficient, scattering coefficient, reduced scattering coefficient, and total attenuation coefficient were calculated as average in the Table II.

Table II.

The calculated microscopic optical properties of agar phantom at around maximum absorbance peak.

Phantom	Absorption Coefficient, μ_a, cm^{-1}	Scattering Coefficient, μ_s, cm^{-1}	Reduced Scattering Coefficient, μ_s', cm^{-1}	Total Attenuation Coefficient, μ_t, cm^{-1}
Agar	0.50 ± 0.08	0.17 ± 0.02	0.02 ± 0.002	0.67 ± 0.06

After optically and acoustically characterizing the phantom and demonstrating that it has a true tissue-like structure, the temperature measurement results can now be given. The temperatures detected by the thermocouples within the agar phantom as a result of the light flushes of the IPL device were found as given in Table III below at different power levels of the device.

Table III.

Temperatures measured in thermocouples as °C inside the agar phantom with the application of different power levels of the IPL light source.

Power Level	1st Thermocouple	2nd Thermocouple	3rd Thermocouple	4th Thermocouple	Average (°C)
1st Power Level	22,40 ± 1,74	22,55 ± 1,92	22,48 ± 2,62	22,45 ± 2,11	22,47 ± 0,06
2nd Power Level	25,07 ± 1,67	25,39 ± 1,82	25,75 ± 2,73	25,56 ± 1,89	25,44 ± 0,29
3rd Power Level	27,21 ± 3,31	27,81 ± 3,72	27,51 ± 5,44	28,10 ± 3,82	27,66 ± 0,38
4th Power level	29,33 ± 1,84	30,10 ± 2,11	30,76 ± 1,25	30,39 ± 1,92	30,15 ± 0,61
5th Power Level	32,56 ± 0,46	33,79 ± 0,76	34,09 ± 1,64	33,21 ± 1,17	33,41 ± 0,68

Average irradiance values calculated at different power levels of IPL device according to 0.80, 0.85, 0.90, .095 and 1.0 emissivity values can be seen between Figure 4 and Figure 8.

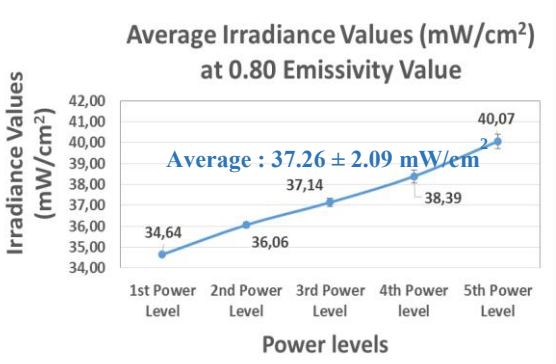

Fig. 4. The average calculated irradiances at 0.80 emissivity value.

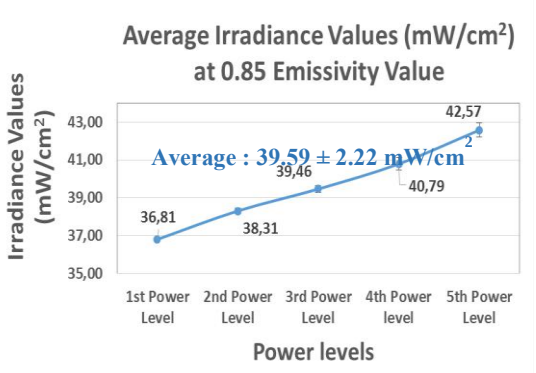

Fig. 5. The average calculated irradiances at 0.85 emissivity value.

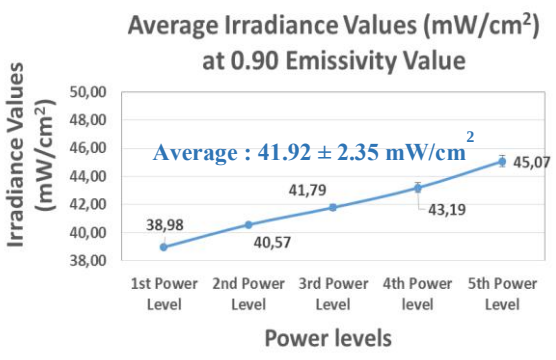

Fig. 6. The average calculated irradiances at 0.90 emissivity value

.

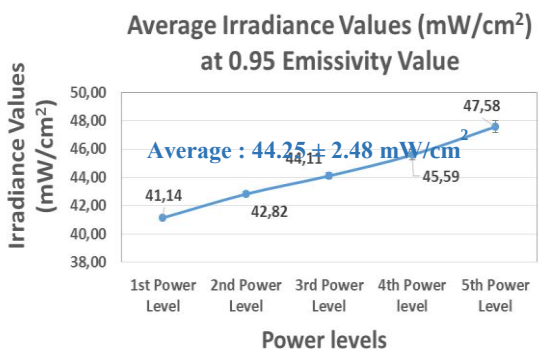

Fig. 7. The average calculated irradiances at 0.95 emissivity value.

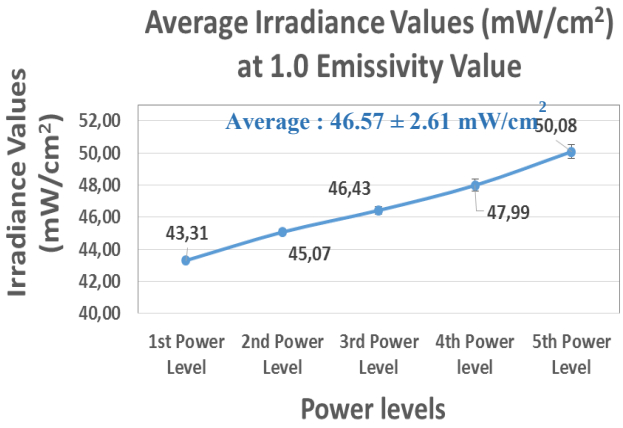

Fig. 8. The average calculated irradiances at 1.0 emissivity value.

The temperatures detected by the thermocouples within the agar phantom as a result of the different lights of the LED device were found as given in Table IV.

Table IV.
Temperatures measured in thermocouples inside the agar phantom with the application of different colors of the LED light source.

LED Color	The Measured Average Temperatures (°C)
Yellow	18,18 ± 0,32
Blue	18,74 ± 0,15
Orange	18,92 ± 0,11
Purple	19,08 ± 0,11
Red	17,21 ± 0,07
Green	17,32 ± 0,06

The irradiance values calculated at different emissivity values from the internal temperatures detected in the agar phantom using the LED therapy device can be seen between Figure 9 and Figure 13.

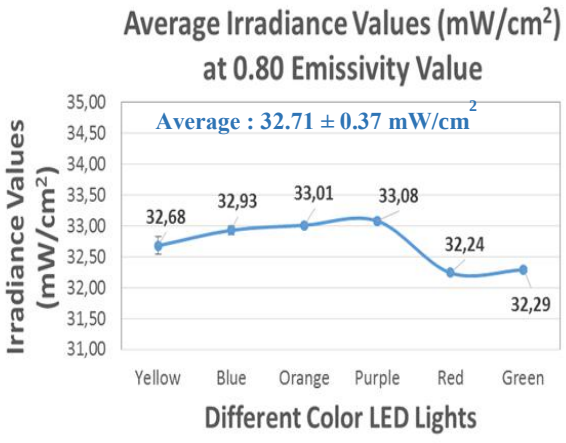

Fig. 9. The average calculated irradiances at 0.80 emissivity value.

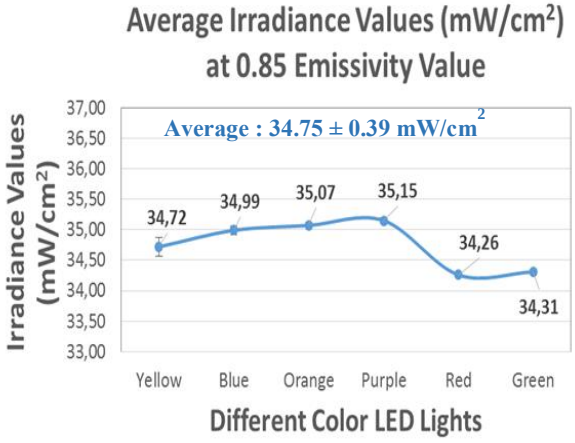

Fig. 10. The average calculated irradiances at 0.85 emissivity value.

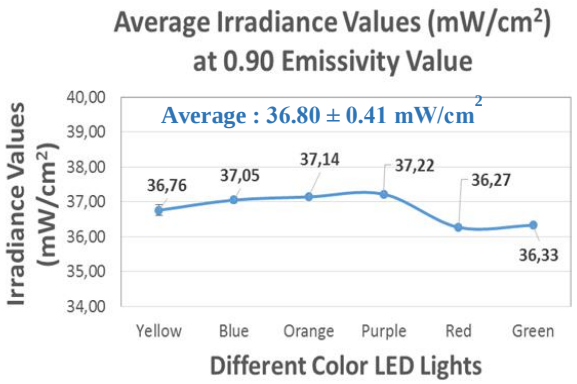

Fig. 11. The average calculated irradiances at 0.90 emissivity value.

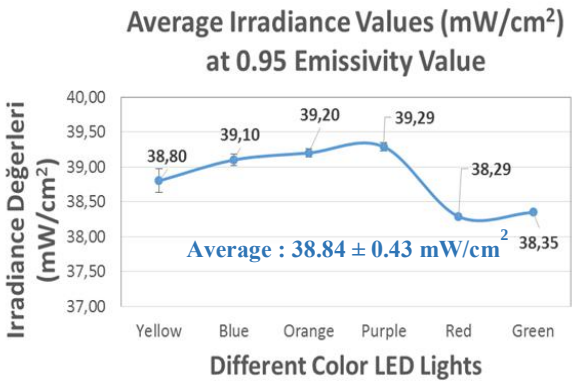

Fig. 12. The average calculated irradiances at 0.95 emissivity value.

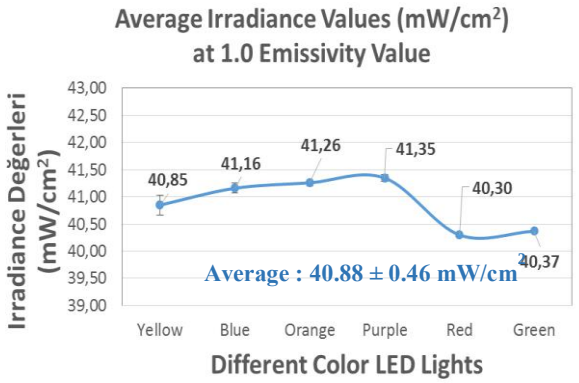

Fig. 13. The average calculated irradiances at 1.0 emissivity value.

The maximum temperatures detected by the thermocouples within the agar phantom as a result of the red color laser application at different time intervals and different distances from the laser source were found as given in Table V.

Table V.

Maximum temperatures measured in thermocouples inside the agar phantom with the application of red laser light source at different time intervals and different distances from the laser source.

The Measured Max. Temperature (°C) at	0 mm	5 mm	10 mm	15 mm	20 mm	25 mm
20 s	22.85	21.45	20.99	21.1	21.24	21.26
40 s	22.88	21.41	21.11	21.2	21.34	21.36
60 s	22.96	21.42	21.19	21.28	21.38	21.41
80 s	23.03	21.44	21.25	21.36	21.43	21.48

The irradiance values calculated at different emissivity values from the internal temperatures detected in the agar phantom using the red color laser can be seen between Table VI and Table X.

Table VI.

Irradiance values calculated for 0.80 emissivity value from the maximum internal temperatures

The Calculated Optical Intensity / Irradiance / Flux Density (mW/cm²) at	0 mm	5 mm	10 mm	15 mm	20 mm	25 mm
20 s	34.82	34.17	33.96	34.00	34.07	34.08
40 s	34.84	34.15	34.01	34.05	34.12	34.13
60 s	34.88	34.16	34.05	34.09	34.14	34.15
80 s	34.91	34.16	34.08	34.13	34.16	34.18

Table VII.

Irradiance values calculated for 0.85 emissivity value from the maximum internal temperatures

The Calculated Optical Intensity / Irradiance / Flux Density (mW/cm^2) at	0 mm	5 mm	10 mm	15 mm	20 mm	25 mm
20 s	37.00	36.30	36.08	36.13	36.20	36.21
40 s	37.01	36.28	36.14	36.18	36.25	36.26
60 s	37.05	36.29	36.18	36.22	36.27	36.28
80 s	37.09	36.30	36.21	36.26	36.29	36.32

Table VIII.

Irradiance values calculated for 0.90 emissivity value from the maximum internal temperatures

The Calculated Optical Intensity / Irradiance / Flux Density (mW/cm^2) at	0 mm	5 mm	10 mm	15 mm	20 mm	25 mm
20 s	39.18	38.44	38.20	38.26	38.33	38.34
40 s	39.19	38.42	38.26	38.31	38.32	38.39
60 s	39.23	38.42	38.30	38.35	38.40	38.42
80 s	39.27	38.43	38.34	38.39	38.43	38.46

Table IX.

Irradiance values calculated for 0.95 emissivity value from the maximum internal temperatures

The Calculated Optical Intensity / Irradiance / Flux Density (mW/cm^2) at	0 mm	5 mm	10 mm	15 mm	20 mm	25 mm
20 s	41.35	40.58	40.32	40.38	40.46	40.47
40 s	41.37	40.55	40.39	40.44	40.52	40.53
60 s	41.41	40.56	40.43	40.48	40.54	40.55
80 s	41.45	40.57	40.47	40.53	40.56	40.59

Table X.

Irradiance values calculated for 1.0 emissivity value from the maximum internal temperatures

The Calculated Optical Intensity / Irradiance / Flux Density (mW/cm^2) at	0 mm	5 mm	10 mm	15 mm	20 mm	25 mm
20 s	43.53	42.71	42.45	42.51	42.59	42.60
40 s	43.55	42.69	42.51	42.57	42.65	42.66
60 s	43.59	42.69	42.56	42.62	42.67	42.69
80 s	43.63	42.71	42.60	42.66	42.70	42.73

When the average irradiance values calculated according to different emissivity values over the temperature data found for IPL, LED and laser experiments in the agar phantom, Figure 14 appears. As can be seen in Figure 14, the average irradiance values increase as the emissivity value increases. In other words, the irradiance value is directly dependent on the emissivity value. Therefore, it must be determined precisely.

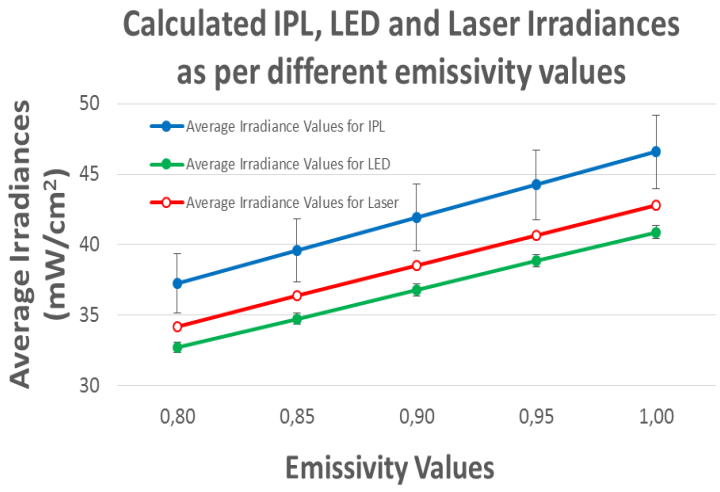

Fig. 14. The calculated IPL, LED and Laser irradiances at different emissivity value.

After determining the irradiance data, energy densities (J/cm^2) can be calculated for different time periods and different emissivity values. For example, energy densities for each light therapy device (IPL, LED and Laser) at 0.9 emissivity value have been calculated as in Fgure 15. In this way, others can be calculated and graphed. So, data of the calculated energy densities of IPL, LED and Laser therapy devices according to the emissivity data for 1 s are given in Table XI below. By the way, we also need to explain why we chose the emissivity coefficient as 0.90. Teper et al. [34], in their study on the agar phantom model, took the emissivity value as 0.8, 0.85, 0.9 and 0.95. They obtained optimum results at 0.95 emissivity value. They explained that this emissivity value was compatible with the emissivity value of water, which was the main construction material of the phantom. Also in a doctoral study made by Sichao Hou, the emissivity value for agarose (the same material we used in our study) was stated that the agarose gel fluctuates at four different emissivity concentrations in the range of 0.88 to 0.92, so they use an average of 0.90 for the agarose gel over the temperature range of 25 to 70 °C [23]. Therefore, we took the emissivity coefficient as 0.90.

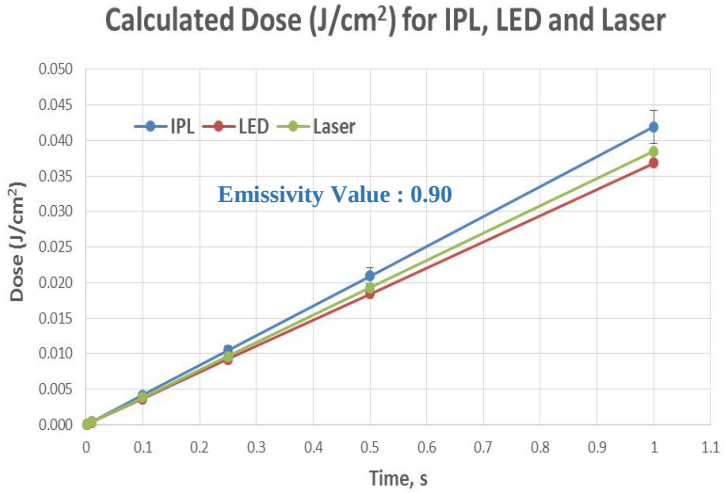

Fig. 15. The calculated energy density of IPL, LED and Laser therapy devices at 0.9 emissivity value.

Table XI.

Energy densities calculated for IPL, LED and Laser for 1 second.

Emissivite Value	Energy Density for IPL (J/cm^2)	Energy Density for LED (J/cm^2)	Energy Density for Laser (J/cm^2)
0.80	0.04 ± 0.002	0.03 ± 0.0004	0.03 ± 0.00004
0.85	0.04 ± 0.002	0.03 ± 0.0004	0.04 ± 0.00004
0.90	0.04 ± 0.002	0.04 ± 0.0004	0.04 ± 0.00004
0.95	0.04 ± 0.002	0.04 ± 0.0004	0.04 ± 0.00004
1.00	0.05 ± 0.003	0.04 ± 0.0005	0.04 ± 0.00005
Average	0.04 ± 0.002	0.04 ± 0.0004	0.04 ± 0.00004

In the literature, there are determined energy densities (fluence) for the treatment of various diseases with light. For example, for open wound healing, this dose value is 2 J/cm^2. Total number of treatments are given as 3-10 times and time interval between treatments are 2-3 days [35]. When we divide 2 J/cm^2 by the values given in Table IX for each emissivity value, we get the durations required to reach 2 J. This value as averages are 48 ± 4.2 s for IPL, 55 ± 4.8 s for LED and 52 ± 4.6 s for laser. The average of all these devices was calculated as 51.7 ± 3.4 s. Again for acne vulgaris, this dose value is given as 2-5 J/cm^2. Total number of treatments are given as 4-10 times and time interval between treatments are 2-3 days. The average times for max. value (5 J/cm^2) are 120.0 ± 10.6 s for IPL, 136.7 ± 12.1 s for LED and 130.7 ± 11.6 s for laser. The average of all these devices for acne vulgaris treatment was calculated as 129.1 ± 8.5 s. For acute pain, this dose value is stated as 5-50 J/cm^2. Total number of treatments are given as every day (new injuries), max 3 days. The average times for max. value (50 J/cm^2) are 1200.2 ± 106.1 s for IPL, 1367.3 ± 120.8 s for LED and 1306.5 ± 115.5 s for laser. The average of all these devices for acne vulgaris treatment was calculated as 1291.4 ± 84.6 s.

CONCLUSION

In conclusion, with this study, it was clearly demonstrated the importance of emissivity coefficient for the irradiance and energy density and thus dose calculations on well-characterized tissue phantom by using light sources having low power intensities. In

addition, it has been shown that emissivity values are very critical in the evaluation of the treatment application times required for the treatment of various diseases with light.

[1] *B. Zhang, X. Huang, S. Huo et al.* Effect of photobiomodulation therapy on mini-implant stability: a systematic review and meta-analysis. Lasers Med Sci 36, 2021. 1557–1566.

[2] *M.A. Vetrici, S. Mokmeli, A.R. Bohm, M. Monici, S.A. Sigman.* 2021. Evaluation of Adjunctive Photobiomodulation (PBMT) for COVID-19 Pneumonia via Clinical Status and Pulmonary Severity Indices in a Preliminary Trial. Journal of inflammation research, 14, 965–979.

[3] *P.G. Vassão, J. Parisi, T.F.C. Penha et al.* Association of photobiomodulation therapy (PBMT) and exercises programs in pain and functional capacity of patients with knee osteoarthritis (KOA): a systematic review of randomized trials. Lasers Med Sci 36, 2021.1341–1353.

[4] *Vinh Van Tran, Minhe Chae, Ju-Young Moon, Young-Chul Lee.* Light emitting diodes technology-based photobiomodulation therapy (PBMT) for dermatology and aesthetics: Recent applications, challenges, and perspectives, Optics & Laser Technology, Volume 135, 2021, 106698.

[5] *H. Shojaei, Y. Sokhangoei, M.R. Soroush.* 2008. Low level laser therapy in the treatment of pressure ulcers in spinal cord handicapped veterans living in Tehran. Iranian Journal of Medical Sciences, 33(1), 44-48.

[6] *T. Bavaresco, A.D.F. Lucena.* 2021. Low-laser light therapy in venous ulcer healing: a randomized clinical trial. Revista brasileira de enfermagem, 75.

[7] *R.K. Mathur, K. Sahu, S. Saraf, P. Patheja, F. Khan, P.K. Gupta.* 2017. Low-level laser therapy as an adjunct to conventional therapy in the treatment of diabetic foot ulcers. Lasers in medical science, 32 (2), 275-282.

[8] *J. Verbelen.* 2007. Use of polarised light as a method of pressure ulcer prevention in an adult intensive care unit. Journal of wound care, 16,4, 145-150.

[9] *H.A. Elessawy, W.H. Borhan, N.A. Ghozlan, S.H. Nagib.* 2021. Effect of light-emitting diode irradiation on chronic nonhealed wound after below-knee amputation. The International Journal of Lower Extremity Wounds, 20, 3, 251-256.

[10] *R.M. Ramos, M. Burland, J.B. Silva, L.M. Burman, M.S. Gelain, L. M.Debom, J. Valmier.* 2019. Photobiomodulation improved the first stages of wound healing process after abdominoplasty: an experimental, double-blinded, non-randomized clinical trial. Aesthetic plastic surgery, 43 (1), 147-154.

[11] *I. Frangež, T. Nizič-Kos, H. B. Frangež.* 2018. Phototherapy with LED shows promising results in healing chronic wounds in diabetes mellitus patients: a prospective randomized double-blind study. Photomedicine and Laser Surgery, 36(7), 377-382.

[12] *de Barros Araújo Júnior, R. Gonzaga, I.C.A. Fernandes, G.A. Lima, A.C.G. Cortelazzi, P.S.T. de Oliveira, R.A. Nicolau, R.A.* 2018. Low-intensity LED therapy (λ 640±20 nm) on saphenectomy healing in patients who underwent coronary artery bypass graft: a randomized, double-blind study. Lasers in Medical Science, 33(1), 103-109.

[13] *A.C.G. Lima, G.A. Fernandes, de Barros Araújo, R. Gonzaga, I.C. de Oliveira, R.A. Nicolau, R.A.* 2017. Photobiomodulation (laser and LED) on sternotomy healing in hyperglycemic and normoglycemic patients who underwent coronary bypass surgery with internal mammary artery grafts: A randomized, double-blind study with follow-up. Photomedicine and laser surgery, 35(1), 24-31.

[14] *M.J. Al Abdullah, Y.G. Mahdi.* 2022. Intense pulsed light versus benzoyl peroxide. Journal of Population Therapeutics and Clinical Pharmacology= Journal de la Therapeutique des Populations et de la Pharmacologie Clinique, 28(2), e54-e61.

[15] *W. Oentari, A.R. Sutrisno, N.K. Jusuf, K. Nasution.* 2022. Intense pulsed light (IPL) as adjuvant therapy for acne vulgaris: A case series. Journal of General-Procedural Dermatology and Venereology Indonesia, 175-181.

[16] *A. Deshpande.* 2022. Efficacy & safety of intense pulsed light therapy for unwanted facial hair: a retrospective analysis in skin of color. Journal of Cosmetic and Laser Therapy, 1-6.

[17] *M. Abrouk, J. Dong, J. S. Waibel.* 2022. Medical and aesthetic improvement of photodamaged skin by the combination of intense pulsed light and photodynamic therapy with 10% aminolevulinic acid hydrochloride gel. Lasers in Surgery and Medicine, 54(1), 62-65.

[18] Giannaccare, Giuseppe MD, PhD, FEBOphth*; Pellegrini, Marco MD, FEBOphth†,‡,§; Carnovale Scalzo, Giovanna MD*; Borselli, Massimiliano MD*; Ceravolo, Domenico OD*; Scorcia, Vincenzo MD* Low-Level Light Therapy Versus Intense Pulsed Light for the Treatment of Meibomian Gland Dysfunction, Cornea: February 3, 2022 - Volume - Issue - doi: 10.1097/ICO.0000000000002997

[19] *B. Karaböce, E. Çetin, H.O. Durmuş, M. Özdingiş, H. Öztürk, K. Mahmat, M.A. Güler.* 2018. Investigation of Different TMMs in High Intensity Focused Ultrasound Applications. In 2018 IEEE International Symposium on Medical Measurements and Applications (MeMeA) (s. pp. 1-5). IEEE.

[20] *H.O. Durmuş, S. Kocaata, G. Naz, Çelik, Y.E. Çetin, E. Karaböce, B. Seyidov, M.Y.* 2020, June. Investigation of Basic Optical Properties of Tissue Phantoms Under 635 nm Low-Level Laser

Irradiation. In 2020 IEEE International Symposium on Medical Measurements and Applications (MeMeA) (pp. 1-6). IEEE.

[21] *H.O. Durmuş, E.Ç. Arı, B. Karaböce, M.Y. Seyidov.* 2020. Measurements of temperature and optical power caused by an IPL therapy device on an artificial tissue. Results in Optics, 1, 100001.

[22] *H.O. Durmuş, E. Çetin, E. Demirkıran, B. Karaböce, M.H.Y. Seyidov.* 2019, November. Investigation of the temperature effect of the LED therapy device on tissue-mimicking material. In AIP Conference Proceedings (Vol. 2178, No. 1, p. 030002). AIP Publishing LLC.

[23] *S. Hou.* 2018. Photo-thermally enhanced temperature gradient gel electrophoresis for DNA separation (Doctoral dissertation, Northeastern University).

[24] *M. Wellons.* 2007. The Stefan-Boltzmann Law. Physics Department, The College of Wooster, Wooster, Ohio, 44691.

[25] https://heliotherapyreviews.com/red-light/red-light-therapy-dosingguide/

[26] *M.Y. Nadeem, W. Ahmed.* 2000). Optical properties of ZnS thin films. Turkish Journal of Physics, 24(5), 651-659.

[27] *D.T. Harvey.* 2003. Analytical Chemistry for Technicians (3rd Edittion b.). John Kenkel.

[28] *S. Chang, A.K. Bowden.* 2019. Review of methods and applications of attenuation coefficient measurements with optical coherence tomography. Journal of biomedical optics, 24(9), 090901.

[29] *J.O. Torrent, V. Barrón.* 2008. Diffuse reflectance spectroscopy. Methods of Soil Analysis Part 5. Mineralogical Methods, 5, 367-385.

[30] *B.C. Wilson.* 1995. Measurement of tissue optical properties: methods and theories. In Optical-thermal response of laser-irradiated tissue. Springer, Boston, MA.

[31] *E.J. Jeong, H.W. Song, Lee, Y.J. Park, S.J. Yim, M. J. Lee, S.S. Kim, B. K.* 2017. Fabrication and characterization of PVCP human breast tissue-mimicking phantom for photoacoustic imaging. BioChip Journal, 11(1), 67-75.

[32] *T.D. Mast.* 2000. Empirical relationships between acoustic parameters in human soft tissues. Acoustics Research Letters Online, 1(2), 37-42.

[33] *L. Ntombela, B. Adeleye N. Chetty.* 2020. Low-cost fabrication of optical tissue phantoms for use in biomedical imaging. Heliyon, 6(3), e03602.

[34] *M. Tepper, A. Shoval, I. Gannot.* 2015. The effect of geometry on tumor thermal profile and its use in tumor functional state estimation. Journal of biophotonics, 8(3), 258-264.

[35] https://energy-laser.com/guide-lines-for-treatment-with-laser-therapy/

Received: 01.07.2022